nature materials

FOCUS | ARTICLES

PUBLISHED ONLINE: 4 MAY 2014 | DOI: 10.1038/NMAT3960

Rigidity sensing and adaptation through regulation of integrin types

Alberto Elosegui-Artola[1,2], Elsa Bazellières[2], Michael D. Allen[1], Ion Andreu[3], Roger Oria[2], Raimon Sunyer[2], Jennifer J. Gomm[1], John F. Marshall[1], J. Louise Jones[1], Xavier Trepat[2,4,5*] and Pere Roca-Cusachs[2,4*]

Tissue rigidity regulates processes in development, cancer and wound healing. However, how cells detect rigidity, and thereby modulate their behaviour, remains unknown. Here, we show that sensing and adaptation to matrix rigidity in breast myoepithelial cells is determined by the bond dynamics of different integrin types. Cell binding to fibronectin through either $\alpha_5\beta_1$ integrins (constitutively expressed) or $\alpha_v\beta_6$ integrins (selectively expressed in cancer and development) adapts force generation, actin flow and integrin recruitment to rigidities associated with healthy or malignant tissue, respectively. *In vitro* experiments and theoretical modelling further demonstrate that this behaviour is explained by the different binding and unbinding rates of both integrin types to fibronectin. Moreover, rigidity sensing through differences in integrin bond dynamics applies both when integrins bind separately and when they compete for binding to fibronectin.

The rigidity of the extracellular matrix (ECM) determines cell proliferation[1], drives differentiation into different lineages[2], and can induce malignant phenotypes if increased above a certain threshold[3]. To detect rigidity, cells must first mechanically probe the ECM. Different contractile structures that apply forces to the ECM have been proposed to serve that purpose[4–7] and to mediate the complex signalling pathways that depend on substrate rigidity[6,8]. However, the molecular mechanism by which cell–substrate forces detect rigidity and trigger any downstream signalling remains unknown. An appealing hypothesis is that this mechanism could be mediated by the unbinding rates of molecular bonds, which have long been described to be determined by force[9]. Such an effect has indeed been proposed to directly mediate rigidity sensing[7], but the hypothesis remains unproven as the relevant molecular bonds have not been identified. Among the different bonds involved in cell–substrate adhesion, those between integrins and the ECM are particularly promising candidates. Indeed, they provide the main molecular mechanical link between cells and their substrate, and they are affected by substrate rigidity[10]. We thus conjectured that integrins provide a rigidity sensing mechanism through their binding and unbinding rates. Further, given the variety of integrin types and their redundancy in binding partners[11], regulation of integrin types with different binding rates to the same ECM component could provide a simple mechanism of rigidity adaptation.

To test this hypothesis, we focused on two receptors to the ECM protein fibronectin (FN): $\alpha_5\beta_1$ integrin, the main FN receptor, with a very well-characterized interaction[12], and $\alpha_v\beta_6$, expressed selectively in developmental, cancer and wound-healing processes and thus potentially providing an adaptation mechanism[13]. As a cell model we used two immortalized lines of human breast myoepithelial cells[14]: myo β_6 cells, overexpressing β_6 integrins (as occurs in ductal carcinoma *in situ*), and control cells without β_6 overexpression (myo ctrl). Both lines constitutively express $\alpha_5\beta_1$. Those lines were ideally suited to study FN–integrin interactions because adhesion to FN-coated substrates required only $\alpha_5\beta_1$ in myo ctrl cells but was mediated by both $\alpha_5\beta_1$ and $\alpha_v\beta_6$ in myo β_6 cells (Supplementary Fig. 1).

Mechanical response to rigidity

We first used traction force microscopy[15,16] to measure the forces exerted by both cell types on FN-coated polyacrylamide gels of different rigidities calibrated with atomic force microscopy. Cells on all rigidities deformed the gels above noise levels, allowing the measurement of forces (Supplementary Fig. 2). Force generation in myo ctrl cells showed a peak at the stiffness corresponding to healthy breast tissue (~1 kPa, as measured also with atomic force microscopy[17]), decreased for higher stiffness characteristic of malignant tissue[17], and then increased again for stiffness values above 5 kPa (Fig. 1a,b). That behaviour was lost in myo β_6 cells, which showed a monotonic increase in force with stiffness (Fig. 1a,b).

We then carried out several experiments to further explore this mechanical behaviour. First, we checked that the differences between cell lines were caused specifically by $\alpha_v\beta_6$. Indeed, differences were abolished by an $\alpha_v\beta_6$ blocking antibody (Fig. 1c) but unaffected by an isotype control antibody (Supplementary Fig. 3b,c). The other FN receptor known to play a mechanical role, $\alpha_v\beta_3$ (ref. 18) did not significantly affect force generation (Supplementary Fig. 3d,e). Second, we confirmed that the effect of $\alpha_v\beta_6$ was mediated by the bond to FN and not by other possible interactions, because plating cells on substrates coated with collagen (which does not bind to $\alpha_v\beta_6$) eliminated the force differences between cell types (Supplementary Fig. 3f,g). Confirming the specific role of FN, overall forces decreased for both cell types when cells were plated on substrates coated with a lower FN density (Supplementary Fig. 3h,i). However, the relative differences and the rigidity trends were maintained for both cell types. Furthermore,

[1]Centre for Tumour Biology Barts Cancer Institute—a Cancer Research UK Centre of Excellence, Queen Mary, University of London, London EC1M 6BQ, UK, [2]Institute for Bioengineering of Catalonia, 08028 Barcelona, Spain, [3]CEIT and TECNUN (University of Navarra), 20018 Donostia-San Sebastian, Spain, [4]University of Barcelona, 08028 Barcelona, Spain, [5]Institució Catalana de Recerca i Estudis Avançats (ICREA), 08010 Barcelona, Spain.
*e-mail: xtrepat@ub.edu; rocacusachs@ub.edu

NATURE MATERIALS DOI: 10.1038/NMAT3960

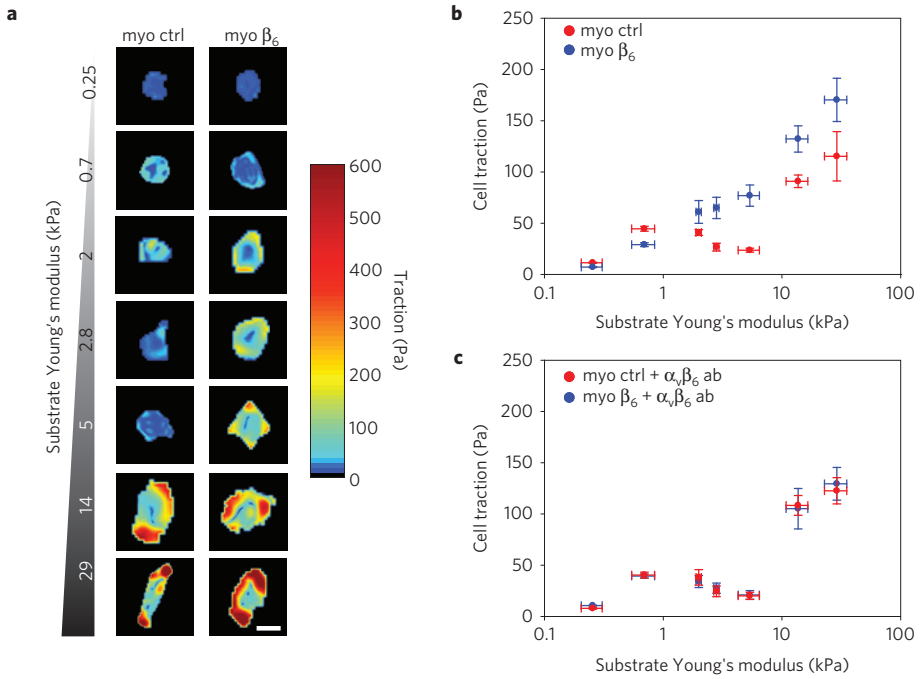

Figure 1 | Expression of $\alpha_v\beta_6$ integrins alters response to substrate stiffness. a, Colour maps showing the traction forces applied by individual myo ctrl or myo β_6 cells on FN-coated polyacrylamide gels of increasing rigidity. Scale bar, 20 μm. **b**, Average forces as a function of rigidity for myo ctrl cells (red) and myo β_6 cells (blue). **c**, Average forces for both cell types after blocking $\alpha_v\beta_6$ with an inhibitory antibody (ab). Differences between cell types were significant without antibodies ($p < 0.05$) but not with antibodies, and the effect of stiffness was significant in all cases ($p < 0.05$). $n \geq 11$ cells per condition. Error bars show standard error of the mean.

performing experiments using culture medium without fetal bovine serum (FBS) did not affect measurements (Supplementary Fig. 3j,k), thereby discarding possible effects of ECM components present in FBS. Other effects due to cell geometry or substrate coating were also ruled out (Supplementary Note 1). Finally, we used primary human breast myoepithelial cells to check that our results were not an artefact of the immortalized myo ctrl and myo β_6 cell lines. Primary cells featured the same behaviour as myo ctrl cells, and the same behaviour as myo β_6 cells after transfecting β_6 integrin (Supplementary Fig. 3l,m). Thus, rigidity sensing by myo β_6 cells was altered by the FN–$\alpha_v\beta_6$ bond, which abolished the local force peak at healthy stiffness present in control cells.

Next, we evaluated whether the different forces exerted by myo ctrl and myo β_6 cells could be due to altered myosin activity. Before plating on the gels, the levels of total myosin light chain and active phosphorylated myosin light chain were the same between cell types (Supplementary Fig. 4a,b). The levels of Rho and Rac, known regulators of contractility and cytoskeletal organization, and of $\alpha_5\beta_1$ integrins, were also the same (Supplementary Fig. 4a,b). Once attached to the gels, myosin phosphorylation moderately decreased for both cell types as rigidity increased, and was slightly higher for myo β_6 cells than myo ctrl cells (Supplementary Fig. 4c,d). The activation of Rho and Rac also exhibited some differences (Supplementary Fig. 4e–h). However, the variations induced by rigidity and cell type in either myosin phosphorylation or Rho/Rac activation did not globally match the corresponding variations measured in forces. Thus, the measured force/rigidity curves could not be explained by biochemical regulation of myosin activity.

Binding dynamics of $\alpha_5\beta_1$ and $\alpha_v\beta_6$ integrins

As regulation of myosin activity could not explain the effect of the FN–$\alpha_v\beta_6$ bond, we then evaluated whether bond dynamics could provide a mechanism. To this end, we first measured the true binding rate (k_{ont}) and unbinding rate (k_{off}) to FN of purified $\alpha_5\beta_1$ and $\alpha_v\beta_6$ integrins using surface plasmon resonance (Fig. 2a). $\alpha_v\beta_6$ integrins had a slightly reduced k_{ont} and strongly increased k_{off} with respect to $\alpha_5\beta_1$ integrins. However, for a given FN molecule on the substrate, actual binding rates to integrins will depend not only on the true binding rate (which defines the probability of binding between two individual molecules), but also on the number of integrins available for binding on the cell membrane. This can be captured by defining an effective binding rate k_{on} as $k_{on} = k_{ont} \cdot d_{int}$, where d_{int} is the density of integrins on the cell membrane[19]. We thus measured integrin densities, which were fivefold higher for $\alpha_v\beta_6$ than for $\alpha_5\beta_1$ (Fig. 2b and Supplementary Fig. 5). As k_{ont} decreased by only half, k_{on} in myo β_6 cells was thus predicted to be higher for $\alpha_v\beta_6$ than for $\alpha_5\beta_1$. To test whether that increase in both k_{on} and k_{off} of $\alpha_v\beta_6$ was observed in cells, we used magnetic tweezers to pull with a constant force on FN-coated beads attached to cells. Consistently with an increase in k_{off}, beads bound to FN through $\alpha_v\beta_6$ (because $\alpha_5\beta_1$ had been blocked) detached faster than beads bound through $\alpha_5\beta_1$ (Fig. 2c and Supplementary Note 2). Those bead-detachment times were not affected by the stiffness of the substrate that cells were on, discarding that downstream processes triggered by rigidity could affect k_{off} (Supplementary Note 2).

Further, the expression of $\alpha_v\beta_6$ reduced the recruitment of $\alpha_5\beta_1$ to FN-coated beads bound to the cell membrane (Fig. 2d,e), but the inverse did not take place (Fig. 2f,g). This shows that $\alpha_v\beta_6$ had a higher affinity for FN than $\alpha_5\beta_1$, indicating that k_{on} had to increase even more than k_{off} to compensate for the increased unbinding (Supplementary Note 2). Thus, in myo β_6 cells and with respect to $\alpha_5\beta_1$, $\alpha_v\beta_6$ had an increased k_{off}, and an even more increased k_{on}.

Rigidity sensing through integrin binding dynamics

We next evaluated how integrin–FN bond dynamics could determine rigidity sensing. As previously proposed in a computational model[7,20], substrate rigidity regulates the loading rate of cell–substrate forces, which in turn determine molecular unbinding rates. This model considers myosin motors pulling on actin filaments, generating the characteristic rearward flow

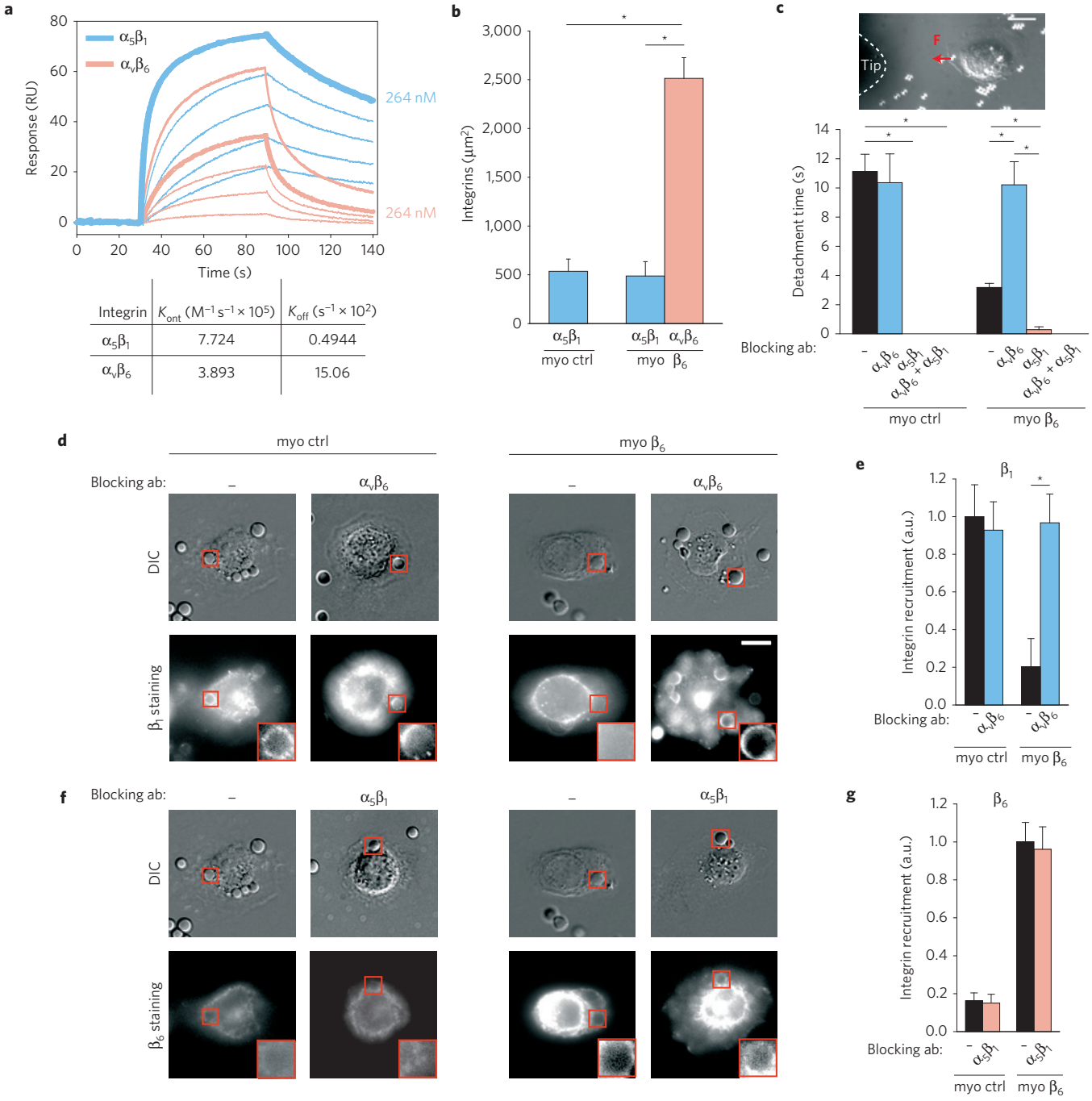

Figure 2 | Both binding and unbinding rates to FN are higher for $\alpha_v\beta_6$ than for $\alpha_5\beta_1$. a, Surface-plasmon-resonance curves showing attachment and subsequent detachment of solutions of purified $\alpha_5\beta_1$ integrins and $\alpha_v\beta_6$ integrins to a FN-coated substrate. Lines of increasing height represent increasing integrin concentrations (9–264 nM for $\alpha_5\beta_1$ and 67–527 nM for $\alpha_v\beta_6$). Data for 264 nM are marked in bold in both cases. Fitted k_{ont} and k_{off} values are shown below the graph ($n \geq 3$ experiments). **b**, Integrin densities on the membrane for both cell types ($n \geq 46$ cells per condition, see also Supplementary Fig. 5). **c**, Top: The tip of a magnetic tweezers device was approached to cells with attached FN-coated magnetic beads, and used to apply a force of 0.5 nN to beads for 2 min. Scale bar, 20 μm. Bottom: Time required to detach beads from myo ctrl or myo β_6 cells (with or without blocking antibodies) after force application ($n \geq 64$ beads from ≥47 cells per condition). **d**, Differential interference contrast (DIC) images and β_1 integrin staining images of myo ctrl or myo β_6 cells (with or without blocking $\alpha_v\beta_6$ integrins) showing β_1 integrin recruitment to FN-coated beads. Insets show beads marked with a red square. **e**, Corresponding quantification of integrin recruitment to beads ($n \geq 20$ beads from ≥10 cells per condition). **f**,**g**, The same as in **d**,**e**, but staining for β_6 integrins and blocking $\alpha_5\beta_1$ integrins instead of the reverse ($n \geq 23$ beads from ≥ 15 cells per condition). Scale bar, 20 μm. *$p < 0.05$. Error bars show standard error of the mean.

of actin towards the cell centre[21]. Actin flow then connects to a substrate of given rigidity through 'clutch' molecules with defined k_{on} and k_{off}. In the filopodia of embryonic chick forebrain neurons, this model successfully predicted traction-force dynamics, as well as the effect of substrate rigidity on the increase of actin speeds and the decrease of traction forces. However, the model did not relate the clutches to specific molecular bonds, and did not include reinforcement, that is, the strengthening and growth of cell–ECM

NATURE MATERIALS DOI: 10.1038/NMAT3960

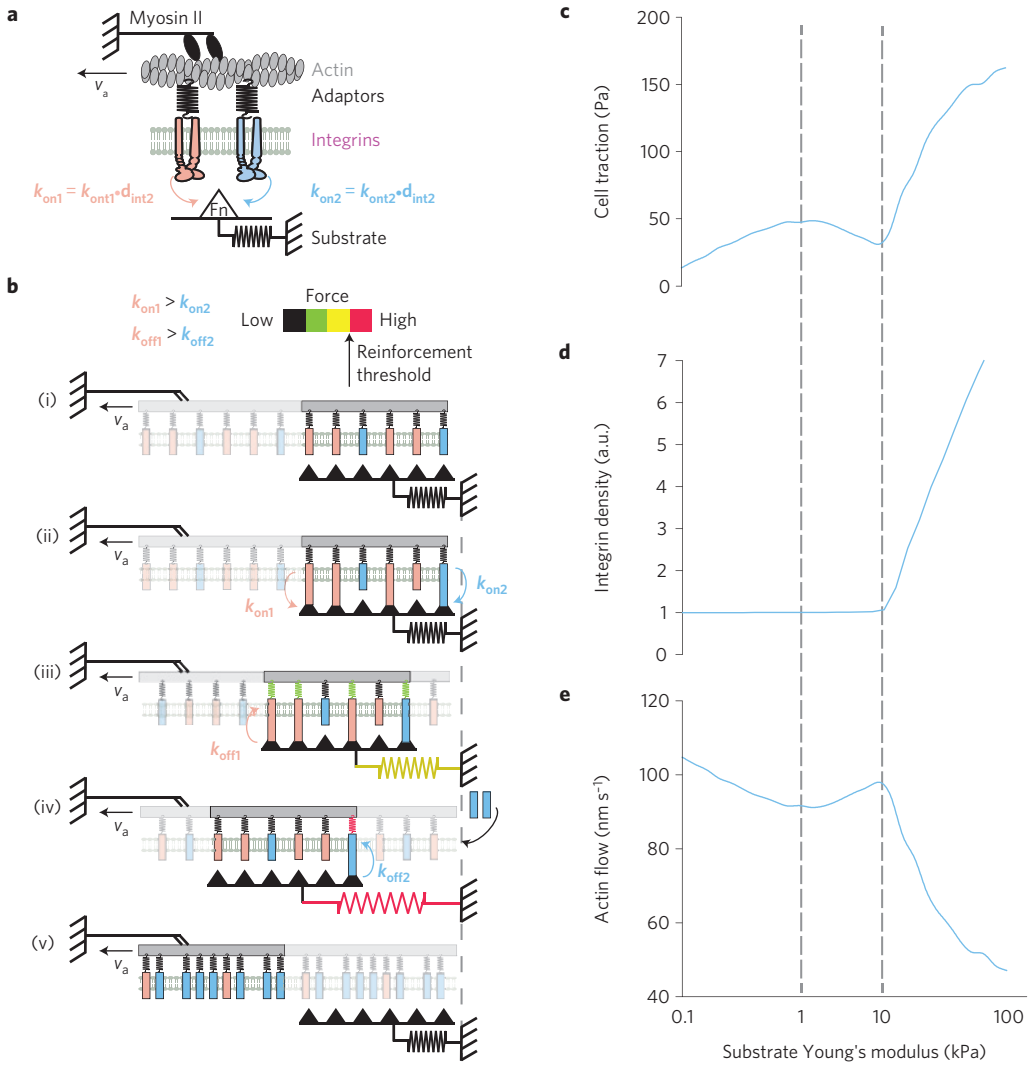

Figure 3 | Integrin–FN clutch model of force transmission. a, Myosin motors pull on actin filaments, which move with rearward speed v_a. Integrins of two different types connect to the actin flow through adaptor proteins, and compete for binding to FN with effective binding rates k_{on1} and k_{on2} given by true binding rates (k_{ont1}, k_{ont2}) multiplied by integrin densities on the membrane (d_{int1}, d_{int2}). FN molecules are in turn connected to a compliant substrate, represented as a linear elastic spring of varying rigidity. **b**, Flow of events (from top to bottom). (i) The model considers a given number of FN molecules (triangles) attached to the substrate, to which integrins can bind. (ii) Orange integrins, with higher k_{on}, will bind faster. (iii) Once they bind, actin rearward movement applies a force on all integrins and the substrate. As orange integrins also have a higher k_{off}, they will detach sooner. (iv) Eventually, blue integrins will detach as well, and if before detaching the force transmitted through them reaches a threshold value, a reinforcement mechanosensing event will result in increased integrin density. (v) Once all integrins detach, force on the substrate is released and the cycle begins again. **c**–**e**, Cell-traction forces (**c**), integrin densities (**d**), and actin speeds (**e**) predicted by the model. The three regimes (separated by dashed lines) are discussed in the main text and in Supplementary Note 4.

adhesions commonly observed after force application in several cell types[18,22]. To address this, we developed a model that expands on one proposed previously[7,20] (see Fig. 3 and Methods for details).

First, we specifically modelled the clutches as FN molecules on the substrate, and the binding and unbinding rates as those between each FN molecule and integrins (Supplementary Note 3). For binding, we considered the effective rate k_{on}, determined by multiplying the true binding rate k_{ont} by the density of integrins d_{int} available for binding to each FN molecule. We also allowed different integrin types (characterized by different k_{on} values) to compete for FN binding (Fig. 3a). For unbinding, we used k_{off} values determined experimentally for the FN–$\alpha_5\beta_1$ single-molecule bond as a function of the applied force[12]. This measured k_{off} depends on force as a catch bond, presenting a maximum stability (minimum k_{off}) at a force of about 30 pN. To allow for possible differences in integrin activation between cell types, we multiplied the k_{off}/force curve by an adjustable scaling factor. In contrast, no experimental data exist for the k_{off}/force curve of single FN–$\alpha_v\beta_6$ bonds. For simplicity and because $\alpha_v\beta_6$ binds to the same RGD motif in FN, unbinding in FN–$\alpha_v\beta6$ bonds was thus modelled simply by changing the scaling factor of the FN–$\alpha_5\beta_1$ k_{off}/force curve. We note, however, that the catch-bond assumption is not essential for model output, and that the same qualitative results can be obtained using slip bonds[7,20]. This could be because under collective loading, catch-bond features may be observable only under uniform bond loading[23,24], which is not the case in a system driven by rearward flow. Finally, as reinforcement was observed in our cells (Supplementary Fig. 6), we included that aspect by increasing integrin density d_{int} by a given amount each time the force in any integrin–FN bond surpassed a certain threshold before breakage (Fig. 3b). This force-sensing event could correspond to force-induced conformational changes in proteins linking integrins to actin[25], exposing binding sites to other

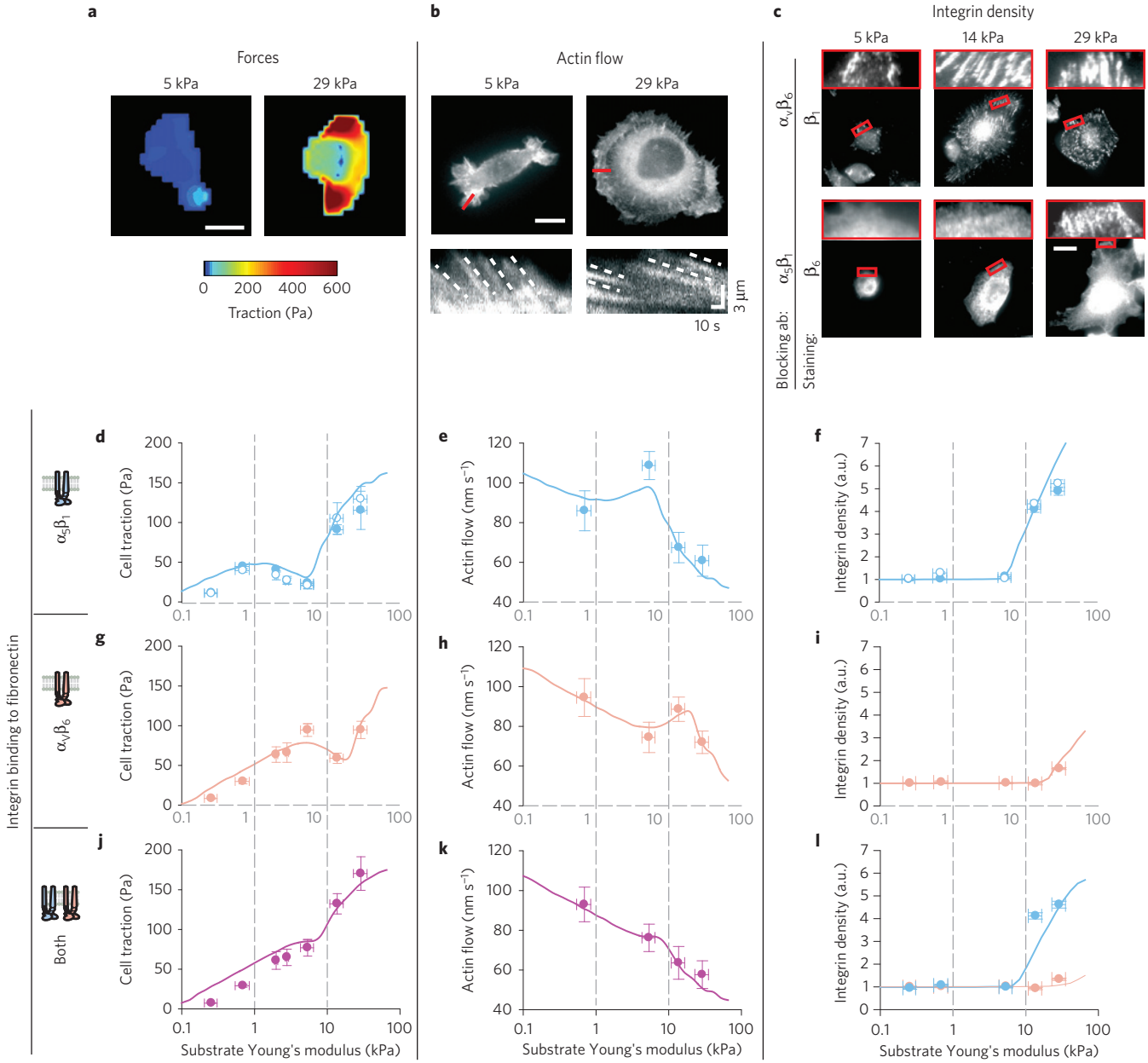

Figure 4 | Integrin–FN binding dynamics predict force generation, actin flow and integrin recruitment in response to substrate stiffness. a, Examples of traction maps exerted by myo ctrl cells plated on substrates of 5 or 29 kPa. **b**, Top: Examples of myo ctrl cells transfected with lifeact–GFP plated on substrates of 5 or 29 kPa. Bottom: Kymographs showing the movement of actin features along the lines marked in red in the top image. The slope of the traces created by the features (marked with dashed lines) was used to calculate actin speed. **c**, Staining of β_1 integrins in myo β_6 cells where $\alpha_v\beta_6$ was blocked, and of β_6 integrins in cells where $\alpha_5\beta_1$ was blocked. Zoomed regions on top of images correspond to rectangles marked in red in the main image. Scale bars, 20 μm. **d**–**l**, For cells on FN-coated gels of varying stiffness, quantifications of average cell traction forces (**d**,**g**,**j**, $n \geq 14$ cells per condition), actin rearward flows (**e**,**h**,**k**, $n \geq 19$ traces from ≥ 7 cells per condition), and integrin densities in adhesions (**f**,**i**,**l**, $n \geq 52$ adhesions from ≥ 10 cells per condition). Results are shown for cells with adhesion mediated by $\alpha_5\beta_1$ integrins (**d**–**f**; filled circle: myo ctrl, open circle: myo $\beta_6 + \alpha_v\beta_6$ ab), $\alpha_v\beta_6$ integrins (**g**–**i**, myo $\beta_6 + \alpha_5\beta_1$ ab), and both integrins (**j**–**l**, myo β_6 cells without any ab). Lines indicate model predictions. In **l**, blue and orange symbols correspond, respectively, to β_1 and β_6 integrin densities. Error bars show standard error of the mean. Statistical analyses are detailed in the Methods.

molecules and providing a mechanotransduction signal to increase integrin concentration.

In essence, substrate rigidity affected the outcome of our model by regulating the rate of force loading experienced by integrin–FN bonds pulled by actin rearward flow. Indeed, the rate at which rearward flow deforms the substrate translates into a small or large rate of force loading depending on whether the substrate is soft or stiff, respectively. Integrin–FN bonds respond to this loading rate, resulting in three regimes as rigidity increases (Fig. 3c). At very low rigidities, force builds so slowly that bonds (which have a non-zero k_{off} even at zero force) detach spontaneously before significant forces can be loaded. In this first regime, increasing loading rates thereby improves force transmission. However, above a certain rigidity loading rates become so high that bonds quickly reach forces where k_{off} increases enough to dominate over k_{on}. In catch bonds, this increase in k_{off} takes place after the force of maximum stability, but the crossover between unbinding and binding dynamics would also happen in a slip bond featuring a monotonic increase of

k_{off} with force. In this second regime, bonds then unbind before allowing time for others to form, decreasing force transmission by reducing the amount of bonds engaged simultaneously. However, as loading rates increase further, unbinding forces in individual bonds (which increase with loading rate) start surpassing the threshold reinforcement force. That increases integrin density and k_{on} (Fig. 3d), leading to a third regime with faster bond formation and improved force transmission. In all cases, transmitted forces pull on and slow actin filaments, leading to an inverse relationship between force and actin rearward flow as previously reported[26] (Fig. 3e and see Supplementary Note 4 for details on model predictions).

To test our model, we first considered the case in which cell–substrate adhesion is mediated by a single integrin type. Using parameters in the range of measured experimental values and a single population of $\alpha_5\beta_1$ integrins (Supplementary Table 1 and Note 5), we were able to capture force generation by cells bound to FN through $\alpha_5\beta_1$ (both myo ctrl cells and myo β_6 cells with $\alpha_v\beta_6$ blocked, Fig. 4d). In contrast, when the same myo β_6 cells bound to FN substrates through $\alpha_v\beta_6$ (because $\alpha_5\beta_1$ had been blocked), the traction peak moved to malignant rigidities (5 kPa, Fig. 4g), and the onset of the third reinforcement regime was delayed. This behaviour was captured by the model after leaving all other parameters constant and increasing only k_{on} (fivefold) and k_{off} (threefold), matching thus the trends in bond dynamics between $\alpha_5\beta_1$ and $\alpha_v\beta_6$ measured in Fig. 2. Thus, simply by binding to FN through integrins with different binding and unbinding rates, cells are able to tune the position of the traction peak. When both integrin types were included (using again the same parameters), the model predicted the monotonic increase in traction force with rigidity that was observed in myo β_6 cells when no integrins were blocked (Fig. 4j and Supplementary Note 4).

We next tested whether our model was able to predict actin flow velocities. To this end, we measured the speed of actin movement in lifeact–GFP-transfected cells, which was higher in cells generating low forces (Fig. 4a,b). When we quantified rearward flow for all conditions, forces and actin speeds were inversely correlated in all cases, with local maxima in forces becoming local minima in speeds and vice versa (Fig. 4e,h,k and Supplementary Movies 1–3). Further, our model quantitatively predicted actin speeds with the same parameters used to predict forces (Fig. 4e,h,k). The model also predicted that the onset of the third regime was associated with an increase in integrin density (Fig. 3d). Indeed, $\alpha_5\beta_1$ and $\alpha_v\beta_6$ integrin densities increased sharply at the points predicted by the model: 14 kPa for $\alpha_5\beta_1$, and 29 kPa for $\alpha_v\beta_6$ (Fig. 4c and Supplementary Fig. 7). A quantitative analysis of integrin densities in adhesions was also in agreement with model predictions in all cases (Fig. 4f,i,l). Thus, bond dynamics to FN were sufficient to explain how $\alpha_5\beta_1$ and $\alpha_v\beta_6$ integrins regulate force generation, actin flow and integrin recruitment in response to substrate rigidity.

Outlook

Different theoretical approaches have been used to propose how the binding dynamics of clustered catch bonds[23,24] could mediate rigidity sensing. Recently, a computational analysis[20] detailed how different parameters, including binding and unbinding rates, could modulate rigidity sensing by molecular clutches driven by rearward flow. However, how this could be achieved experimentally, and what molecules were involved, remained unknown. Our results demonstrate that, by regulating the expression on the membrane of different integrin types, cells can tune their force generation to be optimal at healthy breast tissue stiffness (with $\alpha_5\beta_1$) or malignant stiffness (with $\alpha_v\beta_6$), or to increase monotonically (with both integrins). This rigidity sensing and adaptation emerges naturally from integrin–ECM bond dynamics. Interestingly, integrin bond dynamics also predict the onset of integrin recruitment and subsequent increase in force generation that takes place at high rigidities (the third regime in Fig. 3c–e). In the model, this feature emerges simply after assuming a threshold for force sensing in single mechanosensing molecules, suggesting a mechanism by which cells could couple integrins to mechanosensors sensitive to one mechanical parameter (force) to detect a different mechanical parameter (substrate rigidity). Potentially, such a mechanism could also explain how integrin binding affects a downstream process such as differentiation[27] in a stiffness-dependent manner[10]. Of note, the only effect of force sensing events that we considered was an increase in integrin recruitment, which was sufficient to predict our results. However, additional reported events associated with adhesion formation, such as activation of the FAK–paxillin–vinculin pathway[6], could play synergistic effects by further reinforcing the clutch.

As biological tissues stiffen with force application[28], local force generation maxima provide a homeostatic mechanism: in healthy tissue, a small perturbation tending to increase stiffness would reduce force generation by cells, decreasing tissue stiffness back to the healthy range. In tissue-remodelling scenarios (given by developmental processes, wound healing or cancer), $\alpha_v\beta_6$ recruitment to the membrane would break homeostasis by shifting or eliminating the force peak. Further, because integrin recruitment is triggered by a mechanosensing event after a given stiffness threshold, any process causing a large increase in tissue stiffness beyond this threshold could provide the signal required to break homeostasis.

Methods

Traction-force measurements. For traction-force measurements, cells seeded on gels were placed on an inverted microscope (Nikon Eclipse Ti). Single cells were tracked for 12 h, while we acquired phase-contrast images of the cells and fluorescence images of the embedded nanobeads using a ×40 objective. Then, cells were trypsinized, and an image of bead position in the relaxed state of the gel was acquired. By comparing bead positions with and without cells, a map of gel deformations caused by cells was first obtained using custom particle-imaging-velocimetry software[15]. Then, after assuming that gel displacements were caused by forces exerted by cells in the cell–gel contact area, the corresponding map of cell forces was calculated using a previously described Fourier transform algorithm[16,29]. The average forces per unit area exerted by each cell were then calculated. Force measurements for each cell were taken each hour during the measurement, and the average value for all time measurements was used. Total strain energy exerted by the cells was calculated by performing a scalar product between gel displacement and force for each pixel in the force map, and then adding the result for the entire traction map. Phase-contrast images were also used to calculate average cell-spreading areas as a function of substrate stiffness.

Surface plasmon resonance experiments. True binding rates (k_{ont}) and unbinding rates (k_{off}) were measured using a Biacore T-100 system. First, 82 RU of monomeric biotinylated FN7-10 molecules and biotinylated bovine serum albumin (BSA) molecules were immobilized to flow cells of avidinated sensorchips (Xantec bioanalytics). FN7-10 is a segment of FN responsible for cell binding, and contains the integrin-binding motifs RGD and PHSRN (ref. 30). Then, different concentrations of purified recombinant human $\alpha_5\beta_1$ and $\alpha_v\beta_6$ integrins were diluted in Tris-buffered saline (25 nM Tris and 150 mM NaCl, at pH 7.4) with 1 mM of $CaCl_2$, $MgCl_2$ and $MnCl_2$ to ensure that integrins were in their activated ligand-binding state[31]. Integrin dilutions were then injected at a constant rate of 30 µl min^{-1} for 60 s, followed by an injection of buffer for 60 s. All measurements were taken as the difference between the sensorgrams obtained in the flow cell, with FN7-10 molecules and the reference sensorgrams obtained in the flow cell with biotinylated BSA. The same Tris-buffered saline containing 20 mM EDTA instead of Ca, Mg and Mn ions was used to remove bound integrins and regenerate the surface between measurements. Data were analysed using Scrubber (BioLogic Software) software, and k_{ont} and k_{off} values were obtained after fitting a 1:1 Langmuir binding model.

Magnetic tweezers and bead-recruitment experiments. Magnetic tweezers experiments were carried out as previously described[18,32]. Briefly, carboxylated 3 µm magnetic beads (Invitrogen) were coated with a mixture of biotinylated pentameric FN7-10 and biotinylated BSA (either 1:5 or 1:30). For measurements, cells were first plated on coverslips coated with 40 µ g ml^{-1} laminin (Sigma) to ensure that blocking antibodies used to disrupt adhesion to FN affected only cell–bead and not cell–substrate interactions. FN-coated beads were then

deposited on the coverslips, and attached to cells. The tip of the magnetic tweezers device was then used to apply a force of 0.5 nN for 2 min on beads attached to cell lamellipodia. Then, the percentage of beads still attached to cells after force application was calculated. For beads that detached, the time of force application required for detachment was also calculated. To quantify integrin recruitment to beads, cells attached to FN7-10-coated beads were fixed and stained for β_1 and β_6 integrins as described in the immunostaining section. To avoid the high autofluorescence of magnetic beads, 3 μm carboxylated silica beads (Kisker Biotech) were used. The average fluorescence intensity on the beads and on surrounding areas was then measured, and the difference between both values was taken as a measure of integrin recruitment.

Rearward-flow measurements. To measure actin rearward flow, cells were transfected with lifeact–GFP, lifeact–mRuby or α_5 integrin (courtesy of R. Horwitz[33], Addgene plasmid 15238) using jetPRIME transfection kit (Polyplus transfection) 2 days before measurements. Cells were then plated on gels of varying rigidity, and imaged every second for 2 min with an oil immersion ×100 objective with spinning-disc confocal microscopy (Andor). For each cell, kymographs were obtained at the cell periphery, and actin speed was measured from the slope of actin features observed in the kymographs. In cells plated on 0.25 kPa gels, actin features were so diffuse that no reliable slopes could be measured in kymographs.

Immunostaining. For fluorescence staining of integrins, cells were fixed with 4% paraformaldehyde, permeabilized with 0.1% Triton X-100, and labelled first with primary antibodies (1 h, room temperature), and then with Alexa-conjugated secondary antibodies (Invitrogen) (1 h, room temperature). Fluorescence images were then acquired with a ×60 oil immersion objective (NA 1.40) using a Nikon Eclipse Ti microscope.

Supplementary methods. Cells and reagents, preparation of polyacrylamide gels, measurement of polyacrylamide gel stiffness, adhesion reinforcement measurements, western blotting and Rac/Rho activation measurements, statistical analysis, and the stochastic modelling of traction-force generation are described in the Supplementary Methods.

Received 15 November 2013; accepted 27 March 2014; published online 4 May 2014

References

1. Wang, H. B., Dembo, M. & Wang, Y. L. Substrate flexibility regulates growth and apoptosis of normal but not transformed cells. *Am. J. Physiol. Cell. Physiol.* **279,** 1345–1350 (2000).
2. Engler, A. J., Sen, S., Sweeney, H. L. & Discher, D. E. Matrix elasticity directs stem cell lineage specification. *Cell* **126,** 677–689 (2006).
3. Paszek, M. J. *et al.* Tensional homeostasis and the malignant phenotype. *Cancer Cell.* **8,** 241–254 (2005).
4. Ghassemi, S. *et al.* Cells test substrate rigidity by local contractions on sub-micrometer pillars. *Proc. Natl Acad. Sci. USA* **109,** 5328–5333 (2012).
5. Trichet, L. *et al.* Evidence of a large-scale mechanosensing mechanism for cellular adaptation to substrate stiffness. *Proc. Natl Acad. Sci. USA* **109,** 6933–6938 (2012).
6. Plotnikov, S. V., Pasapera, A. M., Sabass, B. & Waterman, C. M. Force fluctuations within focal adhesions mediate ECM-rigidity sensing to guide directed cell migration. *Cell* **151,** 1513–1527 (2012).
7. Chan, C. E. & Odde, D. J. Traction dynamics of filopodia on compliant substrates. *Science* **322,** 1687–1691 (2008).
8. Schiller, H. B. *et al.* beta1- and alphav-class integrins cooperate to regulate myosin II during rigidity sensing of fibronectin-based microenvironments. *Nature Cell Biol.* **15,** 625–636 (2013).
9. Bell, G. I. Models for the specific adhesion of cells to cells. *Science* **200,** 618–627 (1978).
10. Huebsch, N. *et al.* Harnessing traction-mediated manipulation of the cell/matrix interface to control stem-cell fate. *Nature Mater.* **9,** 518–526 (2010).
11. Humphries, J. D., Byron, A. & Humphries, M. J. Integrin ligands at a glance. *J. Cell Sci.* **119,** 3901–3903 (2006).
12. Kong, F., Garcia, A. J., Mould, A. P., Humphries, M. J. & Zhu, C. Demonstration of catch bonds between an integrin and its ligand. *J. Cell Biol.* **185,** 1275–1284 (2009).
13. Breuss, J. M. *et al.* Expression of the beta 6 integrin subunit in development, neoplasia and tissue repair suggests a role in epithelial remodeling. *J. Cell Sci.* **108,** 2241–2251 (1995).
14. Allen, M. D. *et al.* Altered microenvironment promotes progression of pre-invasive breast cancer: Myoepithelial expression of αvβ6 integrin in DCIS identifies high-risk patients and predicts recurrence. *Clin. Cancer Res.* **20,** 344–357 (2014).
15. Serra-Picamal, X. *et al.* Mechanical waves during tissue expansion. *Nature Phys.* **8,** U628–U666 (2012).
16. Butler, J. P., Tolic-Norrelykke, I. M., Fabry, B. & Fredberg, J. J. Traction fields, moments, and strain energy that cells exert on their surroundings. *Am. J. Physiol. Cell Physiol.* **282,** C595–C605 (2002).
17. Plodinec, M. *et al.* The nanomechanical signature of breast cancer. *Nature Nanotech.* **7,** 757–765 (2012).
18. Roca-Cusachs, P., Gauthier, N. C., del Rio, A. & Sheetz, M. P. Clustering of α5β1 integrins determines adhesion strength whereas αvβ3 and talin enable mechanotransduction. *Proc. Natl Acad. Sci. USA* **106,** 16245–16250 (2009).
19. Litvinov, R. I. *et al.* Resolving two-dimensional kinetics of the integrin alphaIIbbeta3-fibrinogen interactions using binding–unbinding correlation spectroscopy. *J. Biol. Chem.* **287,** 35275–35285 (2012).
20. Bangasser, B. L., Rosenfeld, S. S. & Odde, D. J. Determinants of maximal force transmission in a motor-clutch model of cell traction in a compliant microenvironment. *Biophys. J.* **105,** 581–592 (2013).
21. Hu, K., Ji, L., Applegate, K. T., Danuser, G. & Waterman-Storer, C. M. Differential transmission of actin motion within focal adhesions. *Science* **315,** 111–115 (2007).
22. Riveline, D. *et al.* Focal contact as mechanosensor: Directional growth in response to local strain. *Mol. Biol. Cell* **10,** 341A (1999).
23. sun, L., Cheng, Q. H., Gao, H. J. & Zhang, Y. W. Effect of loading conditions on the dissociation behaviour of catch bond clusters. *J. R. Soc. Interf.* **9,** 928–937 (2012).
24. Novikova, E. A. & Storm, C. Contractile fibers and catch-bond clusters: A biological force sensor? *Biophys. J.* **105,** 1336–1345 (2013).
25. Roca-Cusachs, P., Iskratsch, T. & Sheetz, M. P. Finding the weakest link—exploring integrin-mediated mechanical molecular pathways. *J. Cell Sci.* **125,** 3025–3038 (2012).
26. Gardel, M. L. *et al.* Traction stress in focal adhesions correlates biphasically with actin retrograde flow speed. *J. Cell Biol.* **183,** 999–1005 (2008).
27. Keselowsky, B. G., Collard, D. M. & Garcia, A. J. Integrin binding specificity regulates biomaterial surface chemistry effects on cell differentiation. *Proc. Natl Acad. Sci. USA* **102,** 5953–5957 (2005).
28. Storm, C., Pastore, J. J., MacKintosh, F. C., Lubensky, T. C. & Janmey, P. A. Nonlinear elasticity in biological gels. *Nature* **435,** 191–194 (2005).
29. Roca-Cusachs, P. *et al.* Micropatterning of single endothelial cell shape reveals a tight coupling between nuclear volume in G1 and proliferation. *Biophys. J.* **94,** 4984–4995 (2008).
30. Coussen, F., Choquet, D., Sheetz, M. P. & Erickson, H. P. Trimers of the fibronectin cell adhesion domain localize to actin filament bundles and undergo rearward translocation. *J. Cell Sci.* **115,** 2581–2590 (2002).
31. Shimaoka, M., Takagi, J. & Springer, T. A. Conformational regulation of integrin structure and function. *Ann. Rev. Biophys. Biomol. Struct.* **31,** 485–516 (2002).
32. Roca-Cusachs, P. *et al.* Integrin-dependent force transmission to the extracellular matrix by alpha-actinin triggers adhesion maturation. *Proc. Natl Acad. Sci. USA* **110,** E1361–E1370 (2013).
33. Laukaitis, C. M., Webb, D. J., Donais, K. & Horwitz, A. F. Differential dynamics of alpha 5 integrin, paxillin, and alpha-actinin during formation and disassembly of adhesions in migrating cells. *J. Cell Biol.* **153,** 1427–1440 (2001).

Acknowledgements

We acknowledge support from the Spanish Ministry for Economy and Competitiveness (BFU2011-23111 and BFU2012-38146), a Career Integration Grant within the seventh European Community Framework Programme (PCIG10-GA-2011-303848), the European Research Council (Grant Agreement 242993), the Generalitat de Catalunya, Fundació La Caixa, Fundació la Marató de TV3 (project 20133330), and the Breast Cancer Campaign Tissue Bank. We thank P. Rodríguez, M. Taulés, L. Bardia, M. Rodríguez, V. González, V. Conte, A. Brugués, D. Zalvidea, D. Navajas, A. del Rio and the members of the X.T. and P.R-C. laboratories for technical assistance and discussions.

Author contributions

A.E-A., M.D.A., J.F.M., J.L.J., X.T. and P.R-C. designed research, A.E-A., E.B., I.A., R.O. and R.S. performed experiments, M.D.A., R.S., J.J.G. and P.R-C. contributed new reagents/analytical tools, A.E-A., E.B., M.D.A., J.F.M., J.L.J., X.T. and P.R-C. analysed the data, P.R-C. implemented the computational model, and A.E-A., X.T. and P.R-C. wrote the paper. All authors read the manuscript and commented on it.

Additional information

Supplementary information is available in the online version of the paper. Reprints and permissions information is available online at www.nature.com/reprints. Correspondence and requests for materials should be addressed to X.T. or P.R-C.

Competing financial interests

The authors declare no competing financial interests.